Ecological Modelling 483 (2023) 110425

Contents lists available at ScienceDirect

Ecological Modelling

journal homepage: www.elsevier.com/locate/ecolmodel

# DUET - Distribution of Understory using Elliptical Transport: A mechanistic model of leaf litter and herbaceous spatial distribution based on tree canopy structure

Jenna S. McDanold[a,b,*], Rodman R. Linn[a], Alex K. Jonko[a], Adam L. Atchley[a], Scott L. Goodrick[c], J. Kevin Hiers[d], Chad M. Hoffman[e], E. Louise Loudermilk[c], Joseph J. O'Brien[f], Russell A. Parsons[g], Carolyn H. Sieg[h], Julia A. Oliveto[a]

[a] *Earth and Environmental Sciences Division, Los Alamos National Laboratory, Los Alamos, NM, USA*
[b] *Rochester Institute of Technology, Rochester, NY, USA*
[c] *USDA Forest Service, Southern Research Station, Athens, GA, USA*
[d] *Natural Resources Institute, Texas A&M University, College Station, TX, USA*
[e] *Department of Forest and Rangeland Stewardship, Warner College of Natural Resources, Colorado State University, Fort Collins, CO, USA*
[f] *USDA Forest Service, Forestry Sciences Laboratory, Athens, GA, USA*
[g] *USDA Forest Service, Rocky Mountain Research Station, Fire Sciences Laboratory, Missoula, MT, USA*
[h] *USDA Forest Service, Rocky Mountain Research Station, Flagstaff, AZ, USA*

A R T I C L E I N F O

*Keywords:*
Tree litter
Modeling
Leaves
Needles
Surface fuels
Prescribed fires

A B S T R A C T

Heterogeneity in surface fuels produced by overstory trees and understory vegetation is a major driver of fire behavior and ecosystem dynamics. Previous attempts at predicting tree leaf and needle litter accumulation over time have been constrained in scope to probabilistic models that consider a limited number of key factors influencing tree litter dispersal patterns and decomposition processes. We present a mechanistic model for estimating variation in surface fuels called the Distribution of Understory using Elliptical Transport (DUET). DUET uses a pre-generated voxelated canopy array and distributes the leaf litter from the trees in an elliptical shape based on tree species characteristics, wind data, and location-specific features. DUET then calculates grass growth between trees and around the litter patterns and sets moisture levels based on relative humidity. In this study, we use DUET to simulate spatial distributions of leaf litter and illustrate model sensitivity to several parameters, providing inputs for testing fuel spatial heterogeneity impacts on fire behavior using process-based models.

## 1. Introduction

The spread and intensity of wildland fire is determined by an interplay between elements of the fire environment, including fuels, weather, and topography (Agee, 1996; Rothermel, 1972). Fire behavior sensitivity to fuel heterogeneity depends on fire intensity and qualities of the fire environment. In low wind and low intensity fire scenarios, fire behavior can be particularly sensitive to the distribution of understory or surface fuels, consisting of live herbaceous vegetation, shrubs, and dead leaf litter (Dell et al., 2017; Hiers et al., 2009; Loudermilk et al., 2017; Prior et al., 2018; Stephens et al., 2004). Accounting for the spatial distribution and heterogeneity of surface fuels is thus important for predicting prescribed fire behavior, marginal fire spread, as well as flanking and backing portions of wildfires (Atchley et al., 2021; Campbell-Lochrie et al., 2021; Linn et al., 2021). Recent work has highlighted fire behavior sensitivity to surface fuel distribution for a variety of ecosystems through observation (Loudermilk et al., 2014; O'Brien et al., 2016; Skowronski et al., 2020) and modeling (Coen et al., 2020; Hoffman et al., 2018; Linn et al., 2021; Loudermilk et al., 2011; Parsons et al., 2017).

In addition to wildland fire behavior, tree litter deposition patterns affect ecosystem dynamics by supplying soil nutrients through leaf, bark, and catkin litter decomposition (Midgley et al., 2015). Several studies have examined how different tree species' litter affects soil

* Corresponding author at: Earth and Environmental Sciences Division, Los Alamos National Laboratory, Los Alamos, NM, USA.
*E-mail address:* jennasmcd@lanl.gov (J.S. McDanold).

https://doi.org/10.1016/j.ecolmodel.2023.110425
Received 15 December 2022; Received in revised form 24 May 2023; Accepted 28 May 2023
Available online 2 June 2023

nitrogen and carbon (Lin et al., 2017; Prescott and Grayston, 2013; Trap et al., 2017). More precise representation of spatial litter distributions may lead to a better understanding of ecosystem changes due to litter accumulation from various tree species within forests or wetlands (Stoler and Relyea, 2011), and potentially how patterns of decomposition influence fire effects (Arthur et al., 2012; Carpenter et al., 2020; Stephens et al., 2004).

Heterogeneous tree litter and grass patterns are influenced by various factors, including overstory structure and prevailing winds, which affect when it falls from trees or shrubs, where foliage lands, and how it influences grass distribution and density through indirect effects on resources (Jonard et al., 2006; Pecot et al., 2007; Riegel et al., 1992; Staelens et al., 2003). Once on the ground, other processes redistribute and decompose the litter material (Forrester and Bauhus, 2016; García-Palacios et al., 2016). A number of factors can alter the trajectory of leaves when they fall from the tree, including the shape of the needles or leaves, the height from which they fall, and local winds at the time when they fall (Nickmans et al., 2019). Decay variability, which depends on climatic conditions, species litter characteristics and chemistry, moisture retention, packing density etc., can change the depth and loading of the localized litter accumulation, the nutrient composition of the soils, and the moisture levels present at any given time (Adair et al., 2008; Arthur et al., 2012; Babl-Plauche et al., 2022; Berg and Lönn, 2022; Cornelissen et al., 2017; Keane, 2008; Mitchell et al., 1999).

Traditional sampling methods for obtaining accurate and spatially-explicit estimates of the dynamic heterogeneity of surface biomass require considerable investment in personnel, time, and money (Keane and Reeves, 2012; Tinkham et al., 2012). At stand scales (<100 s of ha), scientists and managers commonly combine surface biomass sampling approaches with other forest and rangeland inventory methods to estimate the fuel load at landscape or prescribed fire burn block scales for various fuel strata (i.e., surface and canopy fuel layers). Terrestrial lidar has been used to characterize more localized (radius of 10 s of m) fuel load in strata (Bright et al., 2017; Jarron et al., 2020; Loudermilk et al., 2009). Lidar techniques and photogrammetric methods (Keane et al., 2012) show success when representing surface fuels (Rowell et al., 2020). However, they are associated with great financial and labor costs when employed at landscape scales (Silva et al., 2016). Aerial lidar can be used at much larger spatial scales, and while it can be used to some degree to map coarse woody debris (Seielstad and Queen, 2003) or shrubs (Gajardo et al., 2014), it is limited in its ability to detect lower strata surface fuels such as litter or grass, due to both signal noise and occlusion. Consequently, most studies using aerial lidar have focused on characterizing the canopy fuel layer and individual tree properties such as tree crown diameter, stem spatial-density, basal area, and biomass in several locations (Goodwin et al., 2006; Hudak et al., 2008; Hyde et al., 2006; Ruiz et al., 2014; Silva et al., 2016). Litter and grass continue to be difficult to map with remote sensing, so spatially explicit data capturing their patterns at large extents is difficult to find.

Most previous work modeling litter dispersal employs probabilistic approaches. Ferrari and Sugita (1996) created an exponential model based on stem location, which Staelens et al. (2003) expanded to include wind influence. Jonard et al. (2006) used a ballistic and a Weibull distribution approach that incorporated height of maximum crown radius, which was also used by Nickmans et al. (2019) to determine soil nutrient characteristics. Linn et al. (2005) used the vertically integrated canopy foliar mass above a location to infer litter and grass patterns, but this approach led to litter being only located directly under trees. The Jonard et al. (2006) model assumed all leaves were released from the center of the tree at the height of maximum crown radius and it modeled leaf dispersal patterns using a seed dispersal model designed by Greene and Johnson (1989). Although there is value in each of these approaches, they miss some of the processes that impact litter dispersal, such as variation in heights and locations of trees from which leaves and needles fall, species-specific leaf and needle characteristics, and dominant seasonal wind events, which can create direction bias in litterfall heterogeneity.

Here, we describe a mechanistic model called the Distribution of Understory using Elliptical Transport (DUET), using a frequently burned longleaf pine woodland in the southeastern U.S. as a case study. Two tree species with different canopy and leaf shapes (pine needles vs. broad leaves) are used to test the model. DUET uses simplified fall trajectories to determine leaf litter and grass spatial patterns from a given overstory structure with specified wind conditions. For brevity, we define leaf litter as only dead leaves and needles. We propose a methodology to model leaf and needle shedding from trees, accumulation on the surface, decay and compaction over time, and the effects of litter buildup on grass growth. The model uses elliptical dispersal regions to represent the area covered by litter as a function of winds and aerodynamic characteristics of falling foliage, based on surface area and drag coefficients approximated from the average size and shape of an individual leaf. We verified the methodology by testing changes in tree height, size and shape of an average leaf, drag coefficients, and wind variance.

## 2. Methods

### 2.1. Model design

DUET accesses canopy structure data stored in three-dimensional voxelated density arrays and produces a discretized spatially explicit array of litter deposited on the ground resolved at meter scales. The deposition region from a voxel within the tree canopy is an elliptical area defined by gravity, local wind estimates, and aerodynamic drag of the foliage that is falling. Models are then used to account for litter decay and compression effects according to each species' characteristics, and grass growth is predicted based on tree shade and litter cover patterns.

### 2.2. Foliage trajectory and deposition

DUET uses species-dependent foliage bulk density for each canopy location in an explicitly resolved forest, woodland, or shrub layer within the domain of interest as input. Bulk density values are provided in a three-dimensional voxelated array. Such arrays can be developed from field measured or remotely sensed data (Linn et al., 2005; Parsons et al., 2018; Pimont et al., 2016). Voxel size depends on the application, but for the purposes of this work, we choose voxel resolution of 1 or 2 m, depending on the simulation.

We assume that in the absence of wind, the foliage from each voxel falls predominantly downward with some oscillating lateral movement due to its unstable aerodynamics. This lateral movement during the fall creates a cone of flight paths from each canopy location that intersect the ground within a circle of radius, $r_{ground}$, measured in meters. If the ground is flat, $r_{ground}$ represents a minimally sized circular deposition footprint since any other trajectory induced by the presence of wind will be a longer distance with more dispersed patterns. This is not strictly true for sloped ground, which will be addressed in future work.

The radius of the resulting deposition pattern is dependent on the time (in seconds) the leaf requires to fall, $t_{fall}$, and the lateral distance the leaf could travel during that time, assuming minimal wind activity. We assume that the leaf reaches terminal vertical velocity quickly and therefore $t_{fall}$ is defined using the height off the ground, $H_C$, divided by the terminal velocity, $v_{terminal}$; $v_{terminal}$ is dependent on the average mass and surface area for a leaf or needle for each species, $m_{fol}$ and $A_{fol}$, the air density for the area, $\rho_{air}$, the acceleration due to gravity, $g$, and a predefined drag coefficient for the leaves or needles, $C_d$, either from literature or species-specific measurements, if available Eqs. (1) and (2).

$$t_{fall} = \frac{H_C}{v_{terminal}} \tag{1}$$

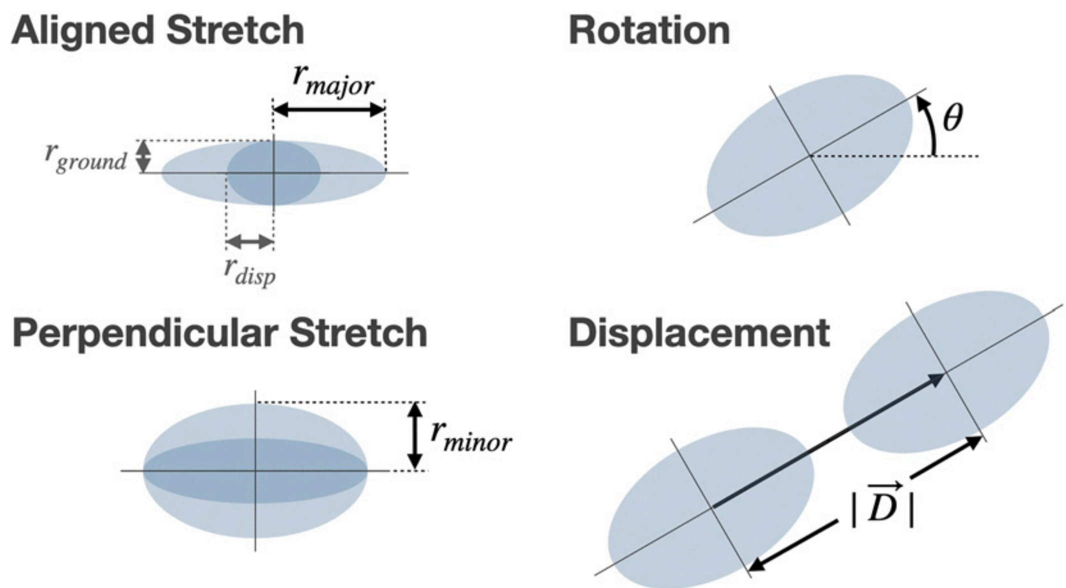


**Fig. 1.** Transformations from wind information for determining dispersal region of leaf or needle fallout; aligned wind stretch is defined using standard deviation multiplied by fall time in the direction of the mean wind trajectory; perpendicular wind stretch is determined by standard deviation multiplied by fall time at 90° to the mean trajectory; rotation and displacement are determined by the mean wind speed trajectory. For more information regarding the elliptical equations defining the dispersal region, please see Appendices A and C.

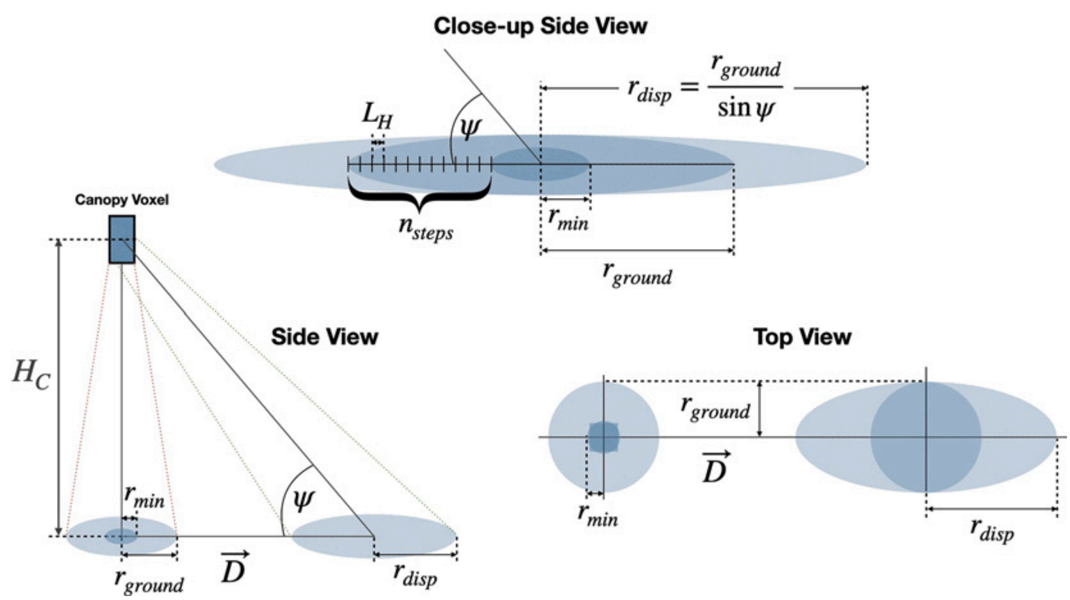


**Fig. 2.** Configuration for the change in major radius of the ellipse when center is displaced.

$$v_{terminal} = \sqrt{\frac{2m_{fol}g}{\rho_{air}A_{fol}C_d}} \tag{2}$$

To calculate $r_{ground}$, we define the effective radius of the voxel of horizontal dimension $dx \times dy$ to be the radius of the deposition circle if the foliage was located just above the ground when it fell, $r_{min} = \sqrt{dxdy/\pi}$. We then add to this minimum radius a distance contributed by oscillating lateral movement, $r_{osc}$, of the foliage as it falls from some height $> 0$:

$$r_{ground} = r_{min} + r_{osc} \tag{3}$$

For information regarding how $r_{osc}$ is defined, please see Appendix A.

Given the circle with radius $r_{ground}$ meters, located at coordinates $(x_c, y_c)$ on the ground below the canopy location, we now perform displacement, stretching, and rotation to this circle to find the dispersal area for the foliage (Fig. 1). These transformations deform the circle into an ellipse centered at $(c_x, c_y)$ with radii $r_{major}$ and $r_{minor}$, aligned along angle $\theta$. To define these transformations, we use mean horizontal wind velocity components in the $x$ and $y$ directions, $u$ and $v$, and their standard deviations, $\sigma_u$ and $\sigma_v$. At the very least, this methodology requires estimates of wind velocities during the time when foliage is falling for each year since the last burn. If more information is available regarding the winds throughout the area, the model allows for the option to separate the year into equal sections (monthly, 4 seasons, 6-months, etc.), each with their own wind velocity components. This offers the opportunity to designate a particular time of year for each specific species to drop their foliage (as different species of trees might drop their foliage at different times of year) and implement related wind conditions for that time.

Using $t_{fall}$, the mean horizontal displacements in the $x$ and $y$ direction, $D_x$ and $D_y$ for the elliptical region can be computed by integrating the horizontal wind velocity over this time. For a discretized spatial and temporal system such as DUET, this collapses to $D_x = u_x t_{fall}$ and

$D_y = u_y t_{fall}$, because of the terminal velocity approximation (gravitational force and drag force are equal) that translates to the foliage moving horizontally as the speed of the surrounding air. See Appendix B for the mathematics of this reduction. By adding components of displacement in the $x$ and $y$ directions, the net average horizontal movement of the foliage can be represented as the vector $\overrightarrow{D} = D_x\overrightarrow{i} + D_y\overrightarrow{j}$ (where $\overrightarrow{i}$ and $\overrightarrow{j}$ indicate the directions aligned with the $x$ and $y$ axes). The displaced center of the elliptical region for dispersal of the leaves or needles, $(c_x, c_y)$, can be computed as $c_x = x_c + D_x$ and $c_y = y_c + D_y$ where $(x_c, y_c)$ is the center of the voxel distributing its leaves.

As the circle is displaced to a new location using $u$ and $v$, the angle of incidence for the cone becomes an ellipse as shown in Fig. 2. The ellipse is now assumed to be aligned such that the major axis is directly in line with the displacement vector, $\overrightarrow{D}$. When the circular cross section with radius $r_{ground}$ of the dispersion path takes on an angular trajectory onto the ground some non-zero horizontal distance from $(x_c, y_c)$, the projected pattern on the ground is much more elliptical in nature. The projected ellipse is modeled with a minor axis that remains $r_{ground}$, and the major axis will be stretched into $r_{disp}$ to account for the angle of incidence fall trajectory and the ground:

$$r_{disp} = \frac{r_{ground}}{\sin\psi} = \frac{r_{ground}\sqrt{H_C{}^2 + \left|\overrightarrow{D}\right|^2}}{H_C} \tag{4}$$

which equals $r_{ground}$ for $\overrightarrow{D} = 0$.

The rotation of the ellipse is determined by calculating the angle between $u$ and $v$ to align it with the displacement vector, $\overrightarrow{D}$ (Fig. 2).

For the two stretches, the standard deviation of the winds directly affects the breadth of the dispersal region. For instance, for high standard deviations in wind direction, the ellipse will be stretched into a broader area than for low standard deviation. This is to account for areas in which vast changes in wind directions occur rapidly during the time when the leaves are falling. See Appendices A and C for more information regarding the mathematical equations used to define these transformations.

### *2.3. Mass dispersal within the elliptical region*

Once the elliptical region is defined, DUET disperses a portion of the mass for each species from a canopy voxel to a particular location in the elliptical region. Each species drops a fraction of the mass within the voxel that is shed per year, $\zeta_{drop}$, or per time period during the year when foliage is shed, $t_{drop}$. $\zeta_{drop}$ is calculated using the inverse of the number of years a species requires to shed its entire canopy, $a_{drop}$; e.g., longleaf pine (*Pinus palustris*) needles are retained for two years (Stowe, 2019). Thus, $a_{drop} = 2$ which makes $\zeta_{drop} = 1/2$ and thus each year 1/2 of the mass within a voxel populated by longleaf pine needles will be dispersed.

As foliage falls along a mean trajectory, we assume that the distribution of the foliage within the deposition region is at its maximum at the center. Since the ellipse defines the outer limit of the potential deviation from the mean fall trajectory the foliage may achieve during its descent, we assume that the deposition load declines linearly from the center to any location on the perimeter of the deposition region. This means that the distribution of the foliage takes on a conical shape, so that the peak of the cone is located at the center of the ellipse, where the mean trajectory intersects the ground, and the distribution reaches zero at the perimeter of the elliptical fall pattern. In the absence of wind, as the dispersal region is circular, this process creates a circular cone distribution; in the presence of a wind field, the cone takes on the elliptical base for surface deposition.

Since the integrated mass over the elliptical area is $\zeta_{drop}$ times the mass within the source canopy cell, $m_c$, we can solve for the maximum mass of the conical distribution, $m_{max}$, which occurs at the center point of the ellipse, $(c_x, c_y)$. We use the equation for the volume of a cone using the elliptical radii, $r_{major}$ and $r_{minor}$:

$$\zeta_{drop} m_c = \frac{1}{3}\pi r_{major} r_{minor} m_{max} \rightarrow m_{max} = \frac{3\zeta_{drop} m_c}{\pi r_{major} r_{minor}} \tag{5}$$

Once the maximum of the conical distribution is known, the deposited mass of the litter at any given point within the elliptical region can be calculated using a linear function with $m_{max}$ as the $y$-intercept. See Section 2.6 for the numerical calculation of the mass dispersal.

For each year since the region was last burned, the elliptical deposition region is identified for foliage falling from all canopy voxels with foliage in them, and the resulting mass depositions are accumulated in appropriate ground-level voxels. This produces a layering effect with each layer tracked separately, representing the litter fall per year within the simulation where total litter load is the sum of the layers in one voxel.

### *2.4. Litter decay*

Decay is an important process controlling litter mass. Olson (1963) illustrates well how variables decay among ecosystems. We postulate that the loss of litter mass accumulated per year, $m_{litter,year}$, with a decay rate for species $s$, $D_{S,year}$, can be written:

$$\frac{\partial m_{litter,year}}{\partial t} = -D_{S,year} m_{litter,year} \tag{6}$$

For mass accumulated in a single year, this becomes

$$m_{litter,year} = \left(1 - e^{-D_{S,year}}\right) m_{litter,year-1} \tag{7}$$

Litter is dispersed per year with various wind conditions, which results in heterogeneous spatial deposition each year. We can imagine this as laying down variably thick litter layers across the forest floor, a layer for each year (or potentially season, depending on the species and location). As annual layers build up in different areas, the decay rate for each of these layers is affected by the number and thickness of layers that have accumulated above it (older layers are likely to have more mass above them). Thus, $D_{S,year}$ might be greater due to moisture retention and compaction when greater mass of litter is stacked above a specific year's layer by litter falling in more recent years (Mueller et al., 2021; Stephens et al., 2004).

For this proof-of-concept demonstration, we approximate the annual decay of *year* layer, $D_{S,year}$, with the most recent year of deposition defined as $Y_r$, with the linear function:

$$D_{S,year} = \sum_{j=year+1}^{Y_r} CP_s m_{litter,j} \tag{8}$$

where $CP_s$ is a species- and area-specific compaction rate, and $m_{litter,j}$ is the mass of the litter deposited in this area during year $j$. Then we have:

$$\frac{\partial m_{litter,year}}{\partial t} = -\left[\sum_{j=iy+1}^{Y_r} CP_s m_{litter,j}\right] m_{litter,year} \tag{9}$$

$$\frac{\partial mass_{accum}}{\partial t} = \frac{\partial \sum_{j=1}^{Y_r} m_{litter,j}}{\partial t} = -\sum_{j=1}^{Y_r}\left[\sum_{k=j+1}^{Y_r} CP_s m_{litter,k}\right] m_{litter,j} + m_{litter,Y_r} \tag{10}$$

There are two long-term effects that result from this increasing decay rate with increasing depth: 1) the rate of change of the litter mass with time since last burn decreases with time and can stop changing when

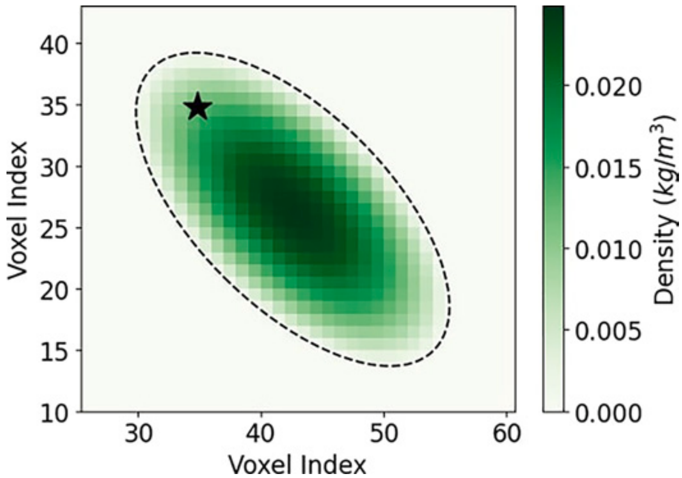


**Fig. 3.** Voxelated density array produced by DUET for use within HIGRAD/FIRETEC fire behavior simulations; the star is the location of a canopy voxel which is located in the 10th vertical cell; wind values used include $u = 9$ m/s, $v = -9$ m/s, $\sigma_u = 5$ m/s, and $\sigma_v = 12$ m/s.

$$\sum_{j=1}^{Y_r}\left[\sum_{k=j+1}^{Y_r} CP_s m_{litter,k}\right] m_{litter,j} = m_{Y_r} \tag{11}$$

and 2) over many years there is an homogenization of litter loads as locations where large amounts of litter falls also eventually gain higher decay rates (Stephens et al., 2004).

### 2.5. Grass production

Grass production is affected by light availability, belowground competition, and inhibition from accumulated tree litter (Hiers et al., 2007; Montgomery et al., 2010; Pecot et al., 2007). The amount of grass is influenced by a litter cover factor $\lambda_l$ (Eq. (11)), determined by the amount of litter covering the ground in a particular voxel, along with a shade factor, $\lambda_s$ (Eq. (12)), determined by the voxel with the maximum density located above the voxel $(x, y)$. Each of these factors are divided by $\rho_{max,species}$, the maximum density of a given species that can exist within a particular voxel.

$$\lambda_l = \frac{\min(\rho_{litter}, \rho_{max,species})}{\rho_{max,species}} \tag{12}$$

$$\lambda_s = \frac{\max_z(\rho_{species,x,y}(z))}{\rho_{max,species}} \tag{13}$$

Once these factors are determined, grass growth is calculated by taking a fraction of the maximum annual grass growth for the area, $grass_{ann,max}$ in mass/year:

$$grass_{x,y} = e^{-(g_l\lambda_l + g_s\lambda_s)} grass_{ann,max} \tag{14}$$

For maximum litter and shade cover, $\lambda_l = \lambda_s = 1$, and Eq. (14) simplifies to $e^{-(g_l+g_s)}$, where $g_l$ and $g_s$ represent the maximum inhibition of grass growth within the given area for litter cover or shade, respectively. Note that if $\rho_{litter}$ and $\max_z(\rho_{species,x,y}(z))$ are equal to 0, we have $e^{-0} = 1$, and there is no reduction in grass growth.

For circumstances in which only the average value of grass growth is known, we normalize these values by finding the average value for the grass across the entire domain using the sum of all of the grass values for every voxel, $grass_{x,y}$, and dividing by the number of cells in the domain, $H_xH_y$, with $H_x$ = total voxels in the domain in the $x$ direction, $H_y$ = total voxels in the domain in the $y$ direction:

$$grass_{x,y} = \frac{\sum_{x,y} grass_{x,y}}{H_xH_y} \tag{15}$$

### 2.6. Numerical implementation

DUET has been designed to create numerical simulations of litter and grass for a designated virtual environment. The inputs for the system include a canopy voxel array and information regarding species and stems per hectare for the area to be simulated. The outputs for the system were designed to be usable by various existing fire or ecosystem models.

#### 2.6.1. Model inputs

DUET simulations begin the year of the last burn, in which the previously existing grass and litter have been consumed, leaving no grass or litter on the ground. This can potentially be adjusted for existing grass and litter in future work. The provided density array for the shrub or canopy fuels that exist in the area, $\rho_f$, must be four-dimensional with three spatial dimensions per species (fourth index is species), assuming no litter or grass. The first layer of this array may contain shrub or canopy fuel, however, as some species stretch into the ground-level voxels (depending on height to foliage on plants and vertical extent of the first cell).

A list of species-specific characteristics, and a list of wind values must also be provided. The species-specific values required include the maximum density of a species, $\rho_{max,species}$, average crown bulk density within the tree, $\rho_{avg}$, an average mass for a single leaf or needle, $m_{fol}$, an average surface area for a single leaf or needle, $A_{fol}$, a drag coefficient for the leaf or needle, $C_d$, a compaction rate, $CP_s$, a moisture level for the live leaf, $M_s$, and a timestep during which the leaves will be dropping from the tree, $t_{drop}$. For instance, the drag coefficient, $C_d$, can be approximated based on the shape of the leaf: a pine needle resembles a thin cylinder which could be approximately $C_d = 0.6$, whereas a broadleaf resembles a piece of paper, which could be approximately $C_d = 2.43$.

Wind information must be provided for the area per time step. Although typically we use year-length time steps, the model can also use shorter time steps to account for the various times during the year that a particular species will lose its canopy. The wind file must list the year, the step during the year, $y_t$, and the corresponding average wind speeds in the $x$ and $y$ directions at canopy height, $u$ and $v$, along with their standard deviations, $\sigma_u$ and $\sigma_v$. These can be directly measured for the area, or obtained from gridded meteorological datasets based either on observations [e.g., Livneh (Livneh et al., 2013) or the Gridded surface Meteorological dataset (Gridmet) (Abatzoglou, 2013)], downscaled climate model simulations [e.g. Multivariate Adaptive Constructed Analogs Comparison Project Phase 5 (MACA CMIP5) (Abatzoglou and Brown, 2012)], or fine-scale atmospheric simulations [e.g. HIGRAD (Dupuy et al., 2011; Koo et al., 2012)]. If a fine-scale atmospheric model is used, the wind field presents as $u$ and $v$ values for each voxel in the domain array based on the vegetation structure itself, and DUET will calculate the $u$, $v$, $\sigma_u$, and $\sigma_v$ values for the vertical column corresponding to the canopy voxel dropping its leaves.

#### 2.6.2. Numerical density calculations

Once the deposition distribution pattern for foliage originating from a particular canopy voxel and species has been defined by the equations in the previous sections, the mass of the foliage is added to the appropriate ground-level voxel. The mass contribution from each canopy or shrub voxel that contains $m_c$ foliage bulk density to each of these ground voxels, $m_{x,y}$, is calculated using a weighting system based on the conical distribution model discussed above:

$$m_{x,y} = \frac{l_n(x,y)}{\sum_{n=1}^{E_n} l_n(x,y)} \zeta_{drop} m_c \tag{16}$$

**Table 1**
Species specific parameters for short versus tall tree simulations.

| | Height (m) | Height to Max crown radius (m) | Canopy Base height (m) | $m_{leaf}$ (g) | $SA_{leaf}$ (cm$^2$) | Decay (%/yr) | Drag Coeff | Compact | Drop per year |
|---|---|---|---|---|---|---|---|---|---|
| Short, Conifer | 10 | 7 | 5.5 | 1 | 0.5 | 1 | 0.6 | 0.2 | 1/2 |
| Tall, Conifer | 20 | 14 | 11 | 1 | 0.5 | 1 | 0.6 | 0.2 | 1/2 |
| Short, Broadleaf | 10 | 0 | 0 | 2.04 | 168 | 0.5 | 2.43 | 0.2 | 1 |
| Tall, Broadleaf | 20 | 0 | 0 | 2.04 | 168 | 0.5 | 2.43 | 0.2 | 1 |

**Table 2**
List of all simulations performed to test various attributes of DUET; PHT = Pine Height, OHT = Oak Height, DCO = Drag Coefficient, DECAY = Decay rate tests, LD = Large Domain, and WFIELD = Windfield; NWNS = No Winds, No Standard deviation; HWNS = High Winds, No Standard deviation; NWHS = No Winds, High Standard deviation; and HWHS = High Winds, High Standard deviation.

| Simulation Name | Perturbed Parameter | Domain Size | m/cell | Trees | Winds (m/s) |
|---|---|---|---|---|---|
| CTH_NWNS | Tree height | 35 × 35 × 25 cells | 1 m | Conifers: 1–10 m, 1–20m | $u, v, \sigma_u, \sigma_v = 0$ |
| CTH_HWNS | Tree height | 35 × 35 × 25 cells | 1 m | Conifers: 1–10 m, 1–20m | $u, v, \sigma_u, \sigma_v = 15, 15, 0, 0$ |
| CTH_NWHS | Tree height | 35 × 35 × 25 cells | 1 m | Conifers: 1–10 m, 1–20m | $u, v, \sigma_u, \sigma_v = 0, 0, 8, 8$ |
| CTH_HWHS | Tree height | 35 × 35 × 25 cells | 1 m | Conifers: 1–10 m, 1–20m | $u, v, \sigma_u, \sigma_v = 15, 15, 8, 8$ |
| BTH_NWNS | Tree height | 35 × 35 × 25 cells | 1 m | Broadleaf: 1–10 m, 1–20m | $u, v, \sigma_u, \sigma_v = 0$ |
| BTH_HWNS | Tree height | 35 × 35 × 25 cells | 1 m | Broadleaf: 1–10 m, 1–20m | $u, v, \sigma_u, \sigma_v = 15, 15, 0, 0$ |
| BTH_NWHS | Tree height | 35 × 35 × 25 cells | 1 m | Broadleaf: 1–10 m, 1–20m | $u, v, \sigma_u, \sigma_v = 0, 0, 8, 8$ |
| BTH_HWHS | Tree height | 35 × 35 × 25 cells | 1 m | Broadleaf: 1–10 m, 1–20m | $u, v, \sigma_u, \sigma_v = 15, 15, 8, 8$ |
| DCO_NWNS | Drag Co = 1.28 and 0.6 | 35 × 35 × 25 cells | 1 m | 2 Identical Conifers | $u, v, \sigma_u, \sigma_v = 0$ |
| DCO_HWNS | Drag Co = 1.28 and 0.6 | 35 × 35 × 25 cells | 1 m | 2 Identical Conifers | $u, v, \sigma_u, \sigma_v = 15, 15, 0, 0$ |
| DCO_NWHS | Drag Co = 1.28 and 0.6 | 35 × 35 × 25 cells | 1 m | 2 Identical Conifers | $u, v, \sigma_u, \sigma_v = 0, 0, 8, 8$ |
| DCO_HWHS | Drag Co = 1.28 and 0.6 | 35 × 35 × 25 cells | 1 m | 2 Identical Conifers | $u, v, \sigma_u, \sigma_v = 15, 15, 8, 8$ |
| DECAY_0.1 | Decay factor = 0.1 | 200 × 200 × 41 cells | 2 m | 2163 trees – Oak and Pine | $u, v, \sigma_u, \sigma_v = 0$ |
| DECAY_0.5 | Decay factor = 0.5 | 200 × 200 × 41 cells | 2 m | 2163 trees – Oak and Pine | $u, v, \sigma_u, \sigma_v = 0$ |
| DECAY_1.0 | Decay factor = 1.0 | 200 × 200 × 41 cells | 2 m | 2163 trees – Oak and Pine | $u, v, \sigma_u, \sigma_v = 0$ |
| WFIELD | Wind field | 200 × 200 × 41 cells | 2 m | 2163 trees – Oak and Pine | Wind field developed in HIGRAD |

$l_n$ is the relative height of the cone distribution pattern within voxel $(x,y)$, and $E_n$ is the total number of surface voxels contained within the entire elliptical deposition region associated with this source canopy voxel. $l_n(x,y)$ is defined as:

$$l_n(x,y) = 1 - \frac{\sqrt{(c_x - x)^2 + (c_y - y)^2}}{\sqrt{(c_x - E_x)^2 + (c_y - E_y)^2}} \tag{17}$$

with $(c_x, c_y)$ as the coordinate of the center of the ellipse and $(E_x, E_y)$ as the corresponding coordinate for the edge of the ellipse such that there exists a straight line that passes through $(c_x, c_y)$, $(x, y)$, and $(E_x, E_y)$. Appendix C fully defines the equations for $E_x$ and $E_y$.

To illustrate how the numerical model applies the conical distribution for a given ellipse, Fig. 3 shows the predicted litter bulk density at each of the surface voxels within the defined elliptical region from a single canopy voxel located 20 m high with wind values of $u = 9m/s$, $v = -9m/s$, $\sigma_u = 5\ m/s$, and $\sigma_v = 12\ m/s$:

## 3. Results

### 3.1. Simulation setup

#### 3.1.1. Tree maps

We consider four synthetic forests to examine the effects on litter dispersal of several species and environmental characteristics including the impact of tree height, drag coefficients, wind influence, average leaf surface area, and decay factors. To show the impact of tree height, we developed two maps with generalized species characteristics (a conifer species and a broadleaf species), each with a single small tree and a single large tree. Table 1 reports the specific measurements used in these short versus tall simulations. Note that the drag coefficients, compaction rates, and drop rates are nondimensional parameters.

These parameter values represent average relative relationships developed from a dataset collected at Eglin Air Force Base in Florida, described in further detail below.

Drag coefficients are used to distinguish fall trajectories for coniferous needles versus broadleaves. We use a drag coefficient of 2.43 for the broadleaf described above, a relatively flat leaf that will have more oscillations due to the larger surface area than the conifer. For a coniferous needle, which has less surface area and therefore will oscillate less as it falls through the air, we use a drag coefficient of 0.6. A map using two identical trees at 10 m tall, 5 m height to maximum crown radius, and 0 m canopy base height with drag coefficients 0.6 and 2.43 compares drag coefficient effects.

We also test the model in a domain populated using tree measurements collected at Eglin Air Force Base in Florida in 2008 (Ottmar et al., 2015), a xeric longleaf pine (*Pinus palustris*) sand-hill forest and grass area with a subtropical climate. The recorded tree locations span an area of approximately 67 m x 106 m. The terrain in this area was without slope at that scale. We used this tree dataset to populate a 400 m x 400 m domain at 2 m lateral resolution using random sampling of the original dataset while preserving measured stem density for a total of 2163 trees in the domain. This dataset included two species of trees: longleaf pine (*Pinus palustris*) and turkey oak (*Quercis laevis*). We used this tree map to test various decay factors and wind field effects.

#### 3.1.2. Wind conditions

To test the effect of winds on the litter deposition, several of the simulations used extreme wind conditions. Using the standard deviation of the winds as a metric for variability, we evaluated four idealized wind scenarios, including (1) a “no wind, no standard deviation” (NWNS) scenario where the litter deposition is solely reliant on height from the tree and atmospheric drag, and represents the circle with radius $r_{ground}$;

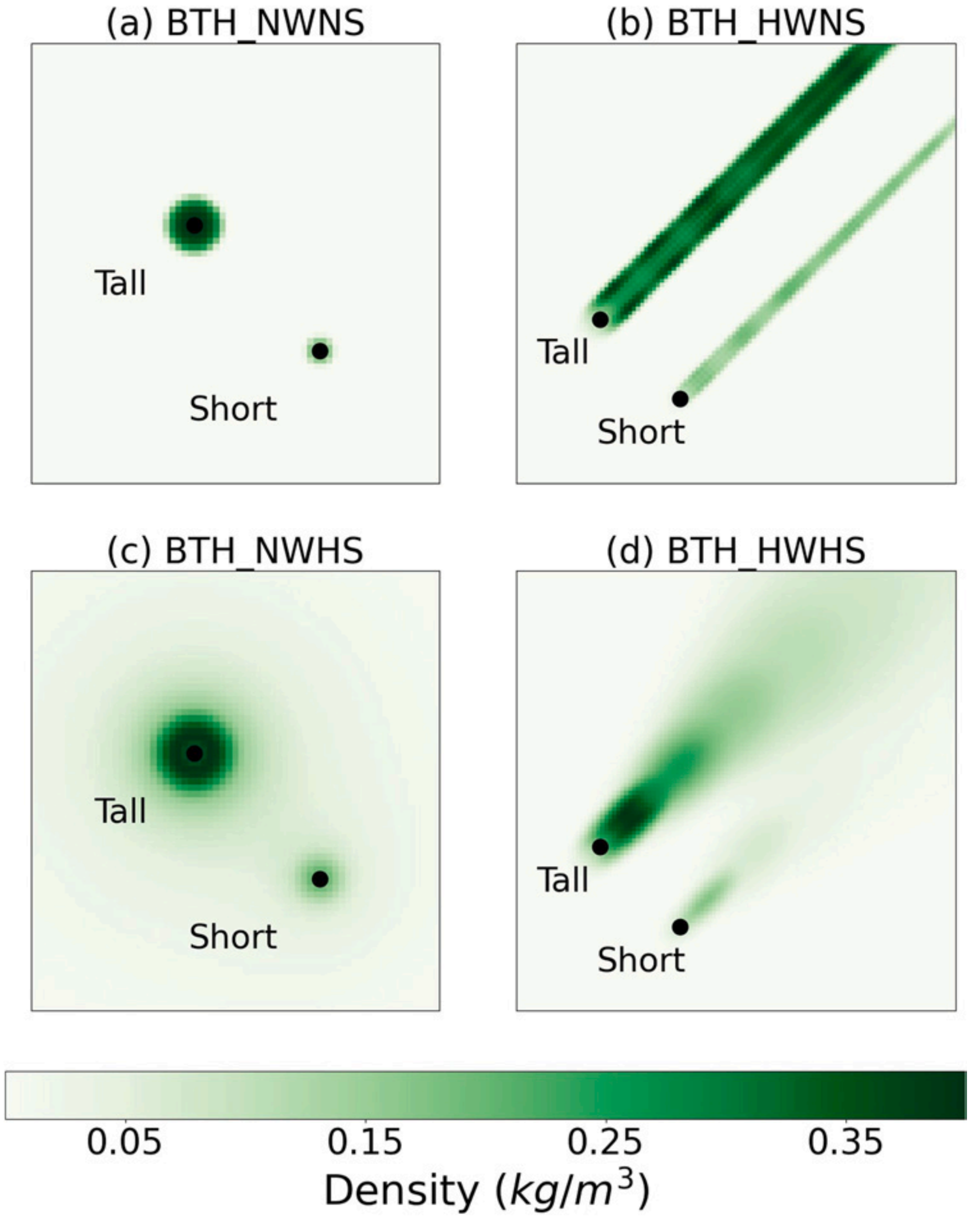


**Fig. 4.** Short versus tall broadleaf tree dispersal for four generalized wind events; a) no wind or standard deviation (NWNS), b) wind at 15 m/s with no standard deviation (HWNS), c) no wind but 8 m/s standard deviation (NWHS), and d) 15 m/s winds with 8 m/s standard deviation (HWHS); BTH = Broadleaf tree height; black dots are tree bole locations.

(2) a "high wind, no standard deviation" (HWNS) scenario with homogeneous strong winds of 15 m/s in every voxel coming directly from the southwest with no standard deviation in trajectory, (3) a "no wind, high standard deviation" (NWHS) scenario where wind speeds average spatially to 0 m/s, but standard deviation is high at 8 m/s in all directions, and (4) a "high wind, high standard deviation" (HWHS) scenario with high average wind speeds (15 m/s), and high standard deviation (8 m/s) in both directions. The simulations in which these wind scenarios are used are described in Table 2.

Then, we examined litter deposition using a more realistic wind profile to incorporate wind gusts that likely cause the leaves to fall from the tree. For this purpose, we first spun up a wind field in HIGRAD using the same Eglin tree plot with a starting wind speed of 13.4112 $m/s$ at a height of 34 m, which is approximately 10 m above the highest tree in the dataset. We used cyclic boundary conditions as described in Pimont et al. (2016). After allowing the wind to find a relatively steady state over 600 s, we then recorded and averaged the mean wind values and variances in each voxel over all time steps to find the average wind speeds and the standard deviation at any given voxel within the three-dimensional domain. We applied DUET using wind information averaged over all voxels from the ground up to the height of the given canopy voxel, $H_C$. The values for the wind scenarios ranged as:

$$1.1872m/s \leq u \leq 13.8865m/s \tag{18}$$

$$-1.04651m/s \leq v \leq 0.9614m/s \tag{19}$$

$$0.0m/s \leq \sigma_u \leq 24.3431m/s \tag{20}$$

$$0.0m/s \leq \sigma_v \leq 7.4149m/s \tag{21}$$

within the areas that contained the canopy voxels. Table 2 includes a list of all the simulations performed to test the functionality of DUET.

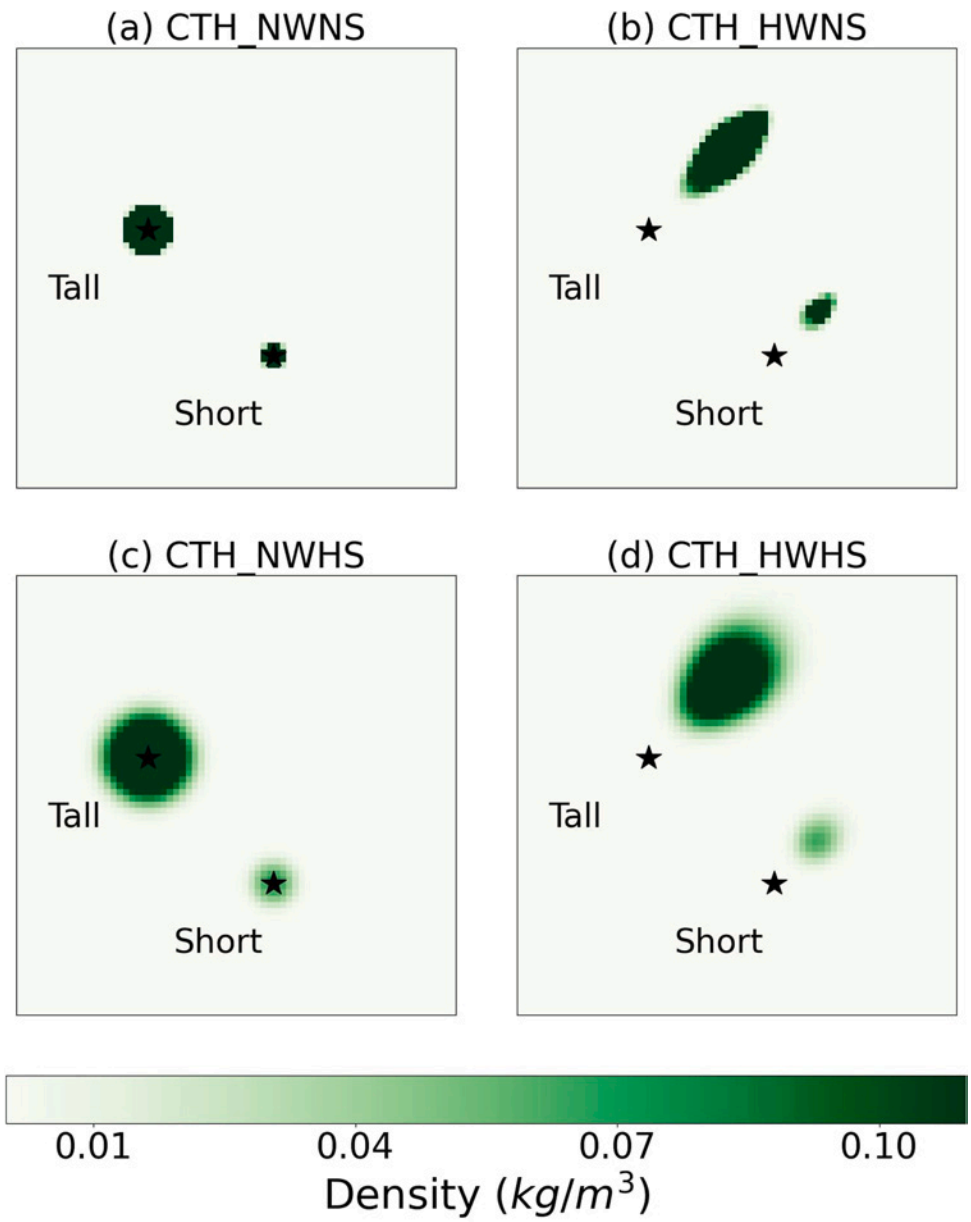


**Fig. 5.** Short versus tall conifer tree dispersal for four generalized wind events; a) no wind or standard deviation (NWNS), b) wind at 15 m/s with no standard deviation (HWNS), c) no wind but 8 m/s standard deviation (NWHS), and d) 15 m/s winds with 8 m/s standard deviation (HWHS); CTH = conifer tree height; black stars are tree bole locations.

### 3.2. Basic model functionality

#### 3.2.1. Effects of tree height

To test the model's ability to distinguish litter dispersal from short versus tall trees, we used a small domain with 1-m resolution and two general tree types, conifer and broadleaf (CTH and BTH simulations described in Table 2). We applied species characteristics as defined in Table 1 in section 2.7.2, with wind descriptions as defined in section 2.7.3 and Table 2. Figs. 4 and 5 show the results of the tree height comparison.

The broadleaf tree canopy represented here stretches down to the ground, while conifer trees have height to live crown distances of 5 m and 10 m for the short and tall trees, respectively. When no mean wind is present, litter accumulates primarily below and around trees. Taller trees result in a broader dispersal area (compare Figs. 4a, 4c, 5a, and 5c). With a positive mean wind, the dispersal area is stretched in the direction of the mean wind. For broadleaf trees, it begins closer to the base of the tree than for the conifer trees (compare Fig. 4b and 4d, and 5b and 5d). Figs. 4c, 4d, 5c, and 5d also show that high wind standard deviations disperse the limited amount of litter from short trees leading to low litter bulk densities in any given voxel.

#### 3.2.2. Drag coefficient comparison

To demonstrate the influence of the drag coefficient on the litter dispersal region, we used a small domain with two trees, each of which were 10 m tall, 5 m maximum radius, 0 m height to live crown, with drag coefficients 0.6 and 2.43. Fig. 6 shows the results of the drag coefficient test.

With the absence of wind influence, the drag coefficient does not affect the dispersal region, as shown in Fig. 6a. A larger drag coefficient expands the dispersal region due to the inverse relationship with terminal velocity, $v_{terminal}$ (Eq. (2)). As $v_{terminal}$ increases, the time it takes for the foliage to fall ($t_{fall}$) increases, which in turn increases the maximum horizontal distance that the foliage can be transported and the greater

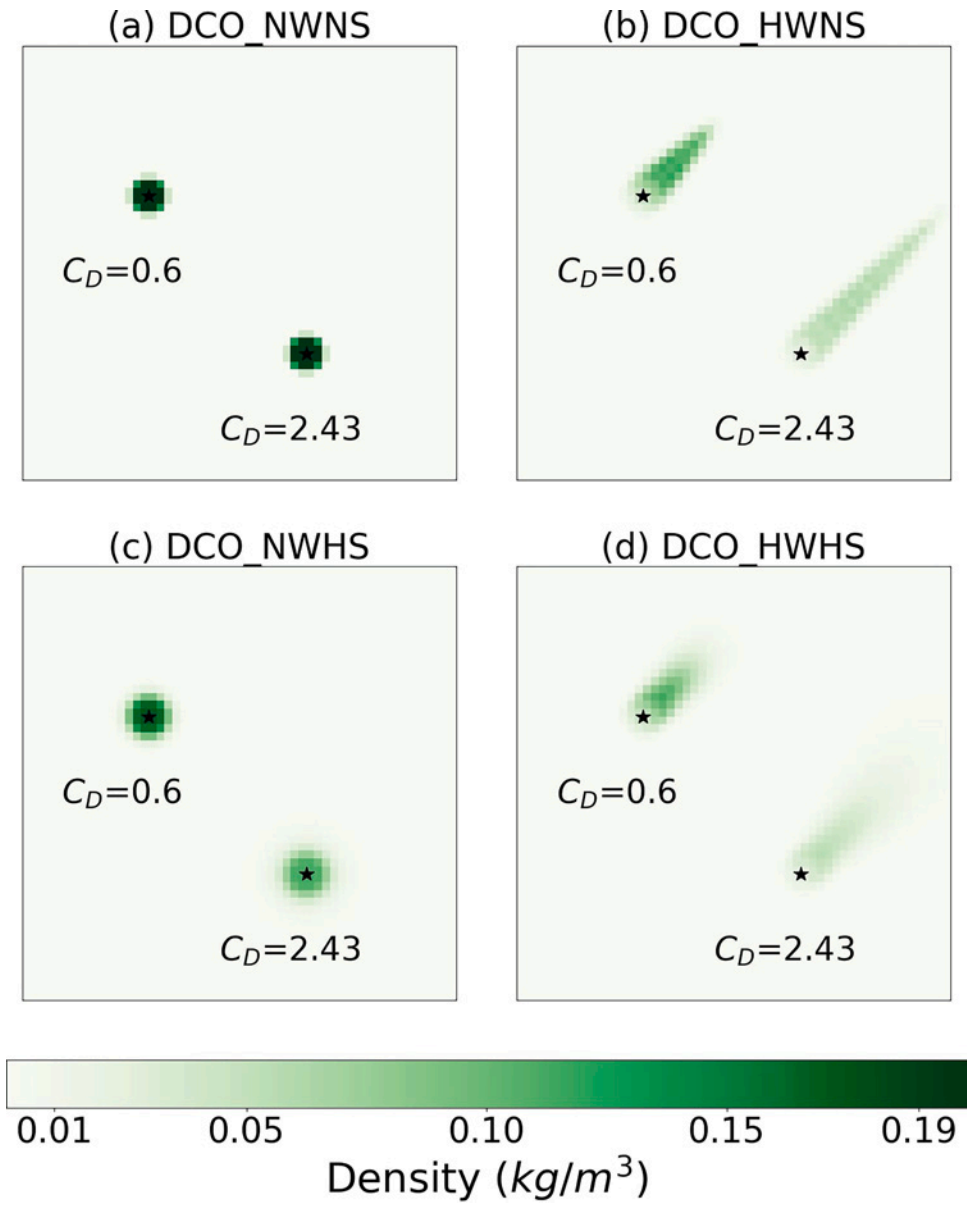


**Fig. 6.** Effect of the Drag Coefficient (DCO) on the dispersal region; all tree characteristics are identical except for the drag coefficient as labelled on the image where one drag coefficient is 2.43 which represents a flat leaf and the other is 0.6 which represents a needle falling; black stars are tree bole locations.

dispersion that can occur, broadening the dispersal region. Fig. 6b-d show these expansions clearly.

#### 3.2.3. *Decay factor comparison*

To show the long-term effects of the decay factor on litter buildup, we ran three five-year simulations on a 400 m x 400 m tree map using the two species described in Table 1. The first simulation tracks how the litter decays when deposited in the first of the five years with no other litter placed for the duration of the simulation (Fig. 7).

To develop Fig. 7, we calculated the litter deposit for a single year with zero wind influence, and then applied the decay function with three different decay factors for 5 years without adding litter after the initial year. With a decay factor of 0.1, we lose $1 - e^{-0.1} \approx 10\%$ of the mass each year; a decay factor of 0.5 results in a loss of $1 - e^{-0.5} \approx 40\%$ mass per year; and a decay factor of 1.0 results in a loss of $1 - e^{-1.0} \approx 63\%$ mass per year. In the figure, we begin with the same amount of litter dispersal for the first year, which is why the litter maps in the column for year 1 are identical.

Since the decay factor of 0.1 only results in 10% loss of mass per year, the mass on the ground remains for several years after the initial dispersal. In Fig. 7, the top row of year 5 is only slightly lighter than the top row of year 1, indicating only a slight loss of mass, or approximately $1 - e^{-0.1(5)} \approx 40\%$ mass loss. In contrast, the decay factor of 1.0 results in a $1 - e^{-1.0(5)} \approx 99\%$ loss of mass over five years, which can be seen in Fig. 7 in the bottom row on the right, which is almost completely devoid of litter.

### 3.3. *Idealized forest area representation*

#### 3.3.1. *Litter buildup under randomized wind conditions*

We performed simulations on a 400 m by 400 m domain with 2 m resolution to examine litter dispersion from trees of variable size and shape. We populated the domain with 2163 trees with heights ranging from 6.7 m to 23.2 m, heights to live crown ranging from 0 m to 17.7 m, and height to maximum crown radius ranging from 1.2 m to 12.8 m. We chose random wind velocities that ranged as:

$$-8.998m/s \leq u \leq 5.308m/s \tag{22}$$

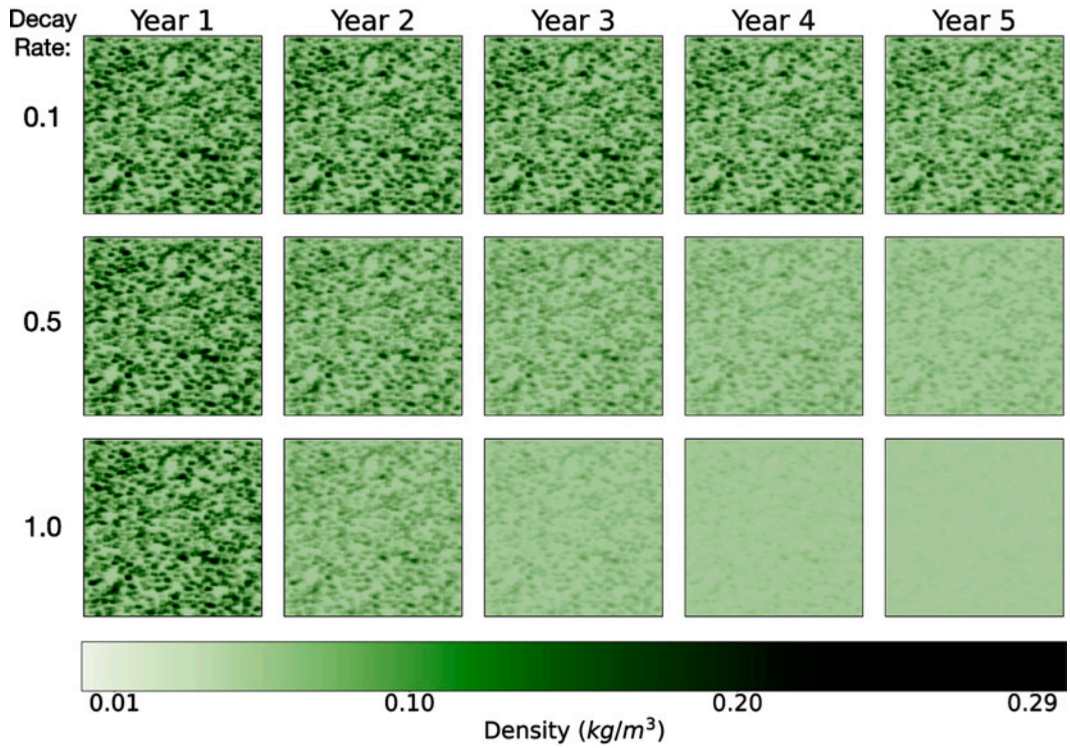


**Fig. 7.** Grass growth through 5 years showing DECAY_0.1 = a decay rate of 0.1 in which there is a 10% loss of mass each year, DECAY_0.5 = a decay rate of 0.5 in which there is a 40% loss of mass each year, and DECAY_1.0 = a decay rate of 1.0 in which there is a 63% loss of mass each year.

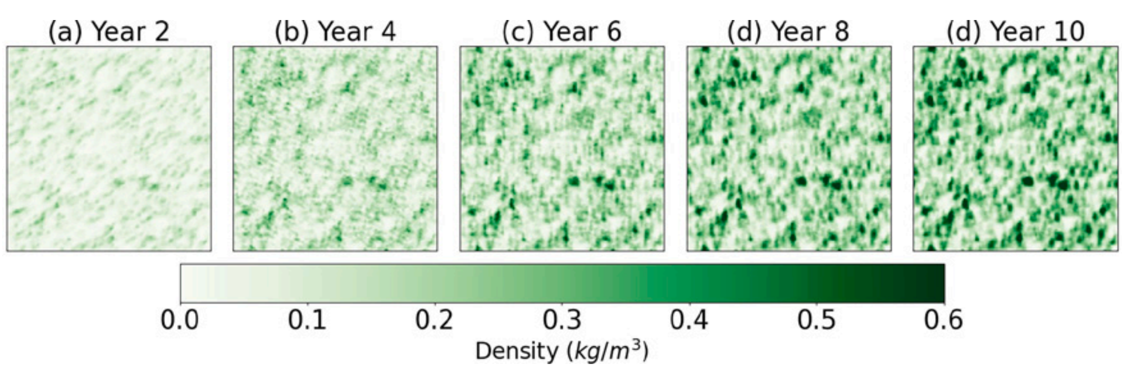


**Fig. 8.** Output for 10 years of litter deposition with random winds to show accumulation of surface litter over time.

$$-8.815m/s \leq v \leq 7.433m/s \tag{23}$$

$$-7.871m/s \leq \sigma_u \leq 8.785m/s \tag{24}$$

$$-7.396m/s \leq \sigma_v \leq 7.330m/s \tag{25}$$

Fig. 8 shows the litter accumulation over ten years with overlapping ellipses. The layering effect for these elliptical dispersal regions is clearly shown in this figure. By year 10, there occurs a clear and direct connection with the canopy structure which is strengthened over time.

### 3.3.2. Litter deposition under gusty wind conditions

Because litter deposition from the canopy is sensitive to the variation in the wind fields, we next explored the influence of variation in winds through the large eddy simulation model HIGRAD, results of which are shown in Fig. 9.

This more realistic wind field represents how we can account for the fully variable wind conditions for each spatial grid cell within the domain. Since the wind fields in these simulations are a function of the stand-scale drag, and include minimal wind speeds close to the ground, we can see that the dispersal regions are restricted closer to the tree locations. Within denser stands, the attenuation of mean windspeed dominates the distribution of litter, with occasional gusts distributing litter farther from originating voxels.

## 4. Discussion

The DUET model can produce a heterogeneous surface litter and grass layer through a mechanistic representation of leaf litter and herbaceous spatial distribution based on tree canopy structure. Simulations explore critical phenomena that lead to the surface fuel deposition and growth patterns, and results agree with expected sensitivities to various canopy and wind parameters. However, there are processes that affect fuel distribution that are not yet included and continued efforts to validate the model are necessary.

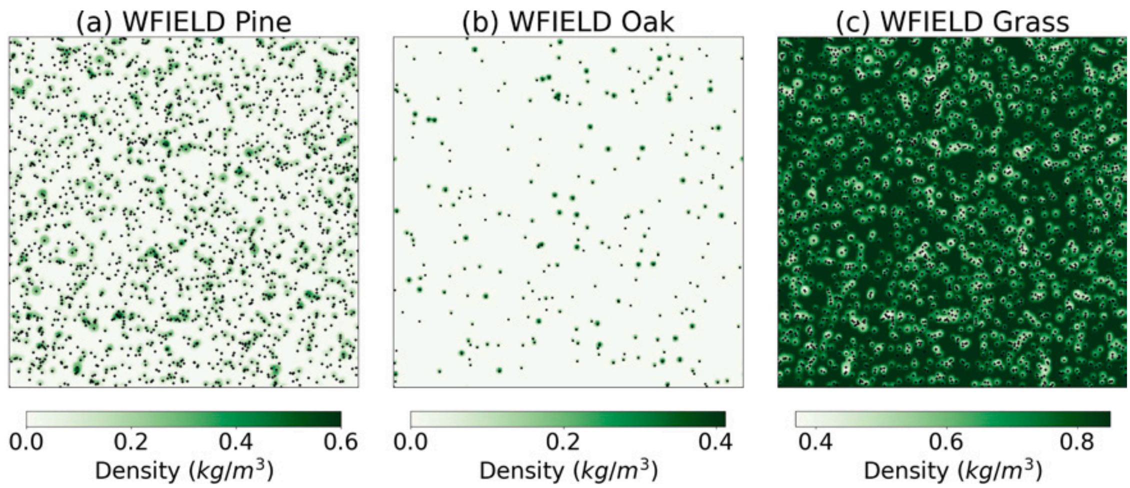


**Fig. 9.** WFIELD simulation; Litter deposition for (a) pine and (b) oak, and (c) grass biomass results from a DUET simulation using wind fields generated by HIGRAD, which captures wind gusts that cause the leaves to detach from the tree.

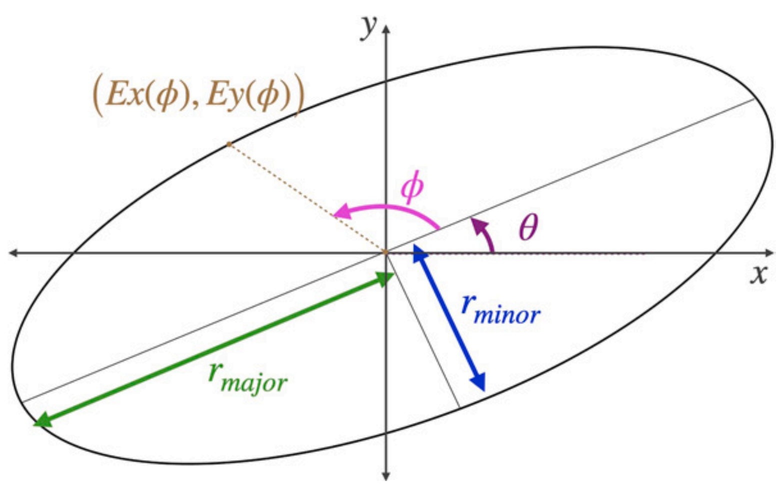


**Fig. C1.** Rotated elliptical region for litter dispersal with $\theta$ = the rotation of the ellipse, $\phi$ defined as all radians between 0 and $2\pi$, $E_x$ and $E_y$ as the displaced coordinates at the specific angle $\phi$, and the radii defined using the wind information in Eqs. A3 and A4.

### *4.1. Overstory structure and composition*

DUET produces modeled tree litter accumulation that is directly affected by overstory structure including the height and species-specific characteristics of the trees, in agreement with observations (Nickmans et al., 2019; Staelens et al., 2003). The model uses the height from which foliage is falling along with the average mass, surface area, and drag coefficient for the foliage (leaves or needles) to calculate the fall time for the foliage based on a terminal velocity approximation. In conjunction with the average wind speeds associated with the time period in which the foliage falls, this fall time helps to define the breadth of the dispersal pattern possible when falling needles or leaves reach the ground. The orientation of the wind-influenced fall path elongates the otherwise circular pattern into an elliptical region if the path is not straight down. Figs. 4 and 5 in Section 3.2.1 show effects of the height of the tree on the deposition region. Species foliage characteristics also influence the width of the deposition pattern. We compare oak leaves, which have a larger surface area and thus greater drag/mass, to pine needles. This slows down the fall speed of oak leaves relative to pine needles, increases the time aloft and allows for more lateral dispersion; therefore, the spread is generally broader for a given tree height (see Fig. 6). Since access to information on canopy structure is more readily available than understory structure, having a model that bases the understory on the canopy may provide the necessary precision for improving fire and ecosystem model inputs (Silva et al., 2016).

### *4.2. Wind influence*

Wind events in the area directly affect when and how the litter falls from the tree (Staelens et al., 2003). In DUET, we use average wind speeds and standard deviations for the area to define the shape and size of the dispersal region. As wind is a main driver for mean horizontal movement of litter while it is falling, we use average wind speed to determine horizontal displacement as well as the orientation, and length of the ellipse in line with the horizontal trajectory. The standard deviation of wind speed affects how wide or narrow the ellipse becomes perpendicular to the displacement vector. We treat the influences of the wind standard deviations as having a diffusion type effect on the leaves or needles, resulting in a conical distribution of leaves when they land. While the majority of the leaves follow the mean path, the net pattern of foliage deposition from any single canopy source is a maximum at the center of the deposition pattern and the loadings fall off to zero linearly at the perimeter. While currently these wind trajectories are static inputs to the model, we hope to connect to a database in which we can implement recorded wind information for various time periods throughout the year and potentially expand DUET to include dynamic wind inputs. Figs. 4, 5, 6, and 9 all show the effect wind conditions have on the elliptical regions and the heterogeneity of the result. In low wind conditions, the dispersal regions remain close to the tree boles, while high wind conditions result in wider spread. Future iterations of the model should incorporate a wind intensity vector that accounts for higher rates of litter drop during high wind events.

### 4.3. Decay processes

Within DUET, decay processes affect how the bulk density, moisture level, and depth of litter changes over the years after deposition, as well as the inhibition of grass growth. With the layering effect created over years of litter accumulation, the decay processes are affected both by species-specific decay factors and depth of litter on top. Fig. 7 shows three different decay factors and the resulting effect on the litter accumulation through the years after they fall. When a smaller decay factor is applied, the litter does not decay and reduce as much as a higher decay factor. When coupled with the layering effect shown in Fig. 8, the decay factor has a high influence on the spatial heterogeneity of litter on the ground over years.

### 4.4. Model assumptions

As with any mathematical model, several assumptions were made within the design of DUET. First, we assumed that leaves reach their terminal vertical velocity immediately during the descent, whereas in reality, the time required to reach terminal velocity is typically reached asymptotically and depends on the air resistance and weight of the object. The latter assumption may be less critical for litter resulting from broad leaves than needles as drag forces lead needles to reach terminal velocity in a shorter time, but a full consideration of velocity is needed in future work.

Further, the decay functions used in DUET are appropriate for shorter timeframes and xeric sites of the southeastern U.S., but don't include nutrient cycling, including carbon:nitrogen, detritivore effects as described in De Smedt et al. (2018) and climatic effects on litter decomposition rates as described in Gavazov (2010). Further expanding the decay function and adding live and dead fuel moisture information, and grass senescence and decay to the model, would improve model accuracy and expand the range of ecosystems to which the model can be applied.

DUET does not currently include redistribution of litter by the wind or animal tracking once on the ground, which is observed predominantly in hardwood litter (Wade and Lunsford, 1989). Many shrub species or trees in shrub stature contribute to the understory characteristics of many surface fire regimes, which are currently included as regular trees but can be added as an additional component to the model.

### 4.5. The need for validation

While the model produces heterogeneity that meets expected patterns for wind, tree height, and litter type, there is a need for both verification and validation. While verification of a model confirms that the model is correctly implemented, validation ensures that the model represents the real system it was built to represent accurately. In this study, we have presented verification of the DUET model by testing the model's representation of various idealized scenarios. However, validation must occur through spatially explicit field data, which are just now becoming available at scales to test DUET (Hawley et al., 2018). As we have worked with various institutions to gather real-world data for validation, we have found that typical methods for collecting data on surface fuels tend to be limited to localized measurements and transect descriptions but lack explicit spatial distribution patterns or spatial correlation with canopy structure or arrangement. We are currently designing a method for collecting data that may more explicitly describe the litter distribution, which should be implemented over the next year. We plan to use this newly developed data set to compare our model to previous models and test for improvement in accuracy. For now, we view DUET as a series of hypotheses that brings together the basic influential processes involved in how the canopy affects litter buildup, which will be evaluated against these high-resolution observations in the future.

## 5. Conclusions

DUET provides complex, realistic and adjustable representations of tree leaf litter and grass distributions that directly relate to canopy structure, litter decay, and wind dynamics. Potential applications of this model include developing realistic heterogeneous surface fuel representations for spatially explicit fire behavior models and ecological examinations of ecosystem dynamics dependent on variable representation of litter biomass (Midgley et al., 2015), including nutrient cycling within senescence processes (Lin et al., 2017; Stoler and Relyea, 2011), and fine scale fire behavior (Hiers et al., 2009). DUET can also be used to examine finer scale litter and grass dynamics that can influence coarser scale fuel and fire dynamics in current stand and landscape level ecosystem models (e.g., Keane et al., 2011; Loudermilk et al., 2011; Scheller et al., 2019).

DUET has the flexibility to be calibrated for any forest type through the tree species characteristics, as well as environmental inputs and parameters. By representing leaf fall within an ellipse, the model allows for approximations within leaf traits, such as surface area and mass, and coarse dispersal functions. Using DUET, one could vary wind speeds and direction through time and characterize several possible surface fuel representations for simulating ecosystem or fire behavior within the area. Our results show how the drag coefficient, wind dynamics, and decay factors affect litter accumulation though space and time. Through species specific parameterization, the model can be calibrated for specific species or generalized for a broad range of species (e.g., conifer vs. broadleaves). Similarly, wind inputs can represent specific wind events or averaged values across a given area. Such mechanistic models are critical for representations of fine scale heterogeneity driven by canopies (Mitchell et al., 2006), their influence on patterns of energy release from fires and resulting patterns of fire effects, as well as ecosystem renewal applications.

## CRediT authorship contribution statement

**Jenna S. McDanold:** Methodology, Software, Validation, Formal analysis, Visualization, Writing – original draft, Writing – review & editing. **Rodman R. Linn:** Conceptualization, Methodology, Validation, Formal analysis, Supervision, Project administration, Funding acquisition, Writing – review & editing. **Alex K. Jonko:** Conceptualization, Methodology, Validation, Formal analysis, Supervision, Writing – review & editing. **Adam L. Atchley:** Conceptualization, Validation, Resources, Writing – review & editing. **Scott L. Goodrick:** Conceptualization, Validation, Resources, Writing – review & editing. **J. Kevin Hiers:** Conceptualization, Validation, Resources, Writing – review & editing. **Chad M. Hoffman:** Conceptualization, Validation, Resources, Writing – review & editing. **E. Louise Loudermilk:** Conceptualization, Validation, Resources, Writing – review & editing. **Joseph J. O'Brien:** Conceptualization, Validation, Resources, Writing – review & editing. **Russell A. Parsons:** Conceptualization, Validation, Resources, Writing – review & editing. **Carolyn H. Sieg:** Conceptualization, Writing – review & editing. **Julia A. Oliveto:** Software, Visualization.

## Declaration of Competing Interest

The authors declare the following financial interests/personal relationships which may be considered as potential competing interests:

JENNA MCDANOLD AND RODMAN LINN has patent pending to LOS

ALAMOS NATIONAL LABORATORY.

**Data availability**

Data will be made available on request.

**Acknowledgements**

This research was supported by the Los Alamos National Laboratory (LANL) through its Laboratory Directed Research and Development (LDRD) program under project number 20220024DR, the USDA Forest Service Rocky Mountain Research Station Interagency Agreement 17-IA-11221633-164, and DoD SERDP projects RC-2643, RC19-21-1119, and RC18-1346. A. Jonko was also supported by LANL LDRD project 20210689ECR. We would like to thank Eglin Air Force Base and Jackson Guard for making longleaf pine data available to us. We thank the USDA Forest Service Southern Research Station and the Athens Prescribed Fire Laboratory in Athens, GA for their support. This research used resources provided by the Los Alamos National Laboratory Institutional Computing Program, which is supported by the U.S. Department of Energy National Nuclear Security Administration under Contract DE-AC52-06NA25396.

**Appendix A**

As described within Section 2.2, to determine $r_{ground}$, we define the effective radius of the voxel of horizontal dimension $dx \times dy$ to be the radius of the circle with equal area to the area of the bottom face of the voxel, $r_{min} = \sqrt{dxdy/\pi}$. We then add a distance contributed by oscillating lateral movement, $r_{osc}$:

$$r_{ground} = r_{min} + r_{osc} \tag{A1}$$

We define $r_{osc} = L_H n_{steps}$, where $L_H$ is found by the Cauchy momentum equation in Lagrangian form. This equation was developed to represent linear transport of a unit of material subjected to the forces acting on the unit as it travels through a given slow-moving fluid. We use this to represent the maximum horizontal distance that the leaf or needle can reach within each oscillation step it takes through the air during its descent. In the model, $L_H$ is calculated by dividing a characteristic length proportional to $\sqrt{A_{fol}}$, where $A_{fol}$ is the surface area of the leaf or needle, by the Froude number, $Fr$, which represents a measurement of buoyancy. To compute the Froude number, we assume minimal oscillation velocity $|u_0| = 0.01$. $n_{steps}$ is the maximum number of steps the leaf or needle can take in the time within which it is falling, $t_{fall}$. We estimate that oscillation frequency of the falling foliage is $N$ steps per second. Definition of this parameter and the proportion constant $a$ could be refined in future work.

$$L_H = \frac{a\sqrt{A_{fol}}}{Fr}, \; Fr = \frac{|u_0|}{\sqrt{g\sqrt{A_{fol}}}}, \; n_{steps} = \left\lceil t_{fall} \times \frac{N\ steps}{s} \right\rceil \tag{A2}$$

The standard deviations of the horizontal wind speeds, $\sigma_u$ and $\sigma_v$, influence the aligned and perpendicular stretches of this displaced ellipse when multiplied by the time for the leaves to fall, $t_{fall}$:

$$r_{major} = r_{disp} + t_{fall}\sigma_u \tag{A3}$$

$$r_{minor} = r_{ground} + t_{fall}\sigma_v \tag{A4}$$

Note that these stretches are mathematically calculated before the rotation of the ellipse. Once the rotation occurs, the stretches are affected by the rotation and are adjusted. In this way, the major and minor axes of the ellipse are affected by both directional wind vectors once the rotation has been applied. See appendix C for more information regarding how the transformations are applied and their resulting equations.

**Appendix B**

We assume that the foliage rapidly reaches the horizontal velocity of the local wind in the $i$ direction, $U_i$, based on its low inertia. With this assumption, the mean horizontal displacement, $D_n$, in the $i$ direction is given by:

$$D_i = \int_0^h U_i(z)\frac{dz}{v_{terminal}} \tag{B1}$$

For scenarios where the average ambient horizontal velocity over the height $h$ is known, the formula collapses to:

$$D_i = \int_0^{t_{fall}} U_i d\tau = U_i t_{fall} \tag{B2}$$

**Appendix C**

In matrix notation, we can use projective coordinates to illustrate the process by which each of the original points within the unit circle move to their new coordinates in the transformed space. In Eq. (C1) the first matrix on the left represents the displacement, the second the rotation, and the third the aligned and perpendicular stretches:

$$\forall\,(x,y)\;\ni\;x^2+y^2\leq 1:\begin{bmatrix}1&0&D_x\\0&1&D_y\\0&0&1\end{bmatrix}\begin{bmatrix}\cos\theta&-\sin\theta&0\\\sin\theta&\cos\theta&0\\0&0&1\end{bmatrix}\begin{bmatrix}r_{major}&0&0\\0&r_{minor}&0\\0&0&1\end{bmatrix}\begin{bmatrix}x\\y\\1\end{bmatrix}=\begin{bmatrix}E_x\\E_y\\1\end{bmatrix}\tag{C1}$$

This series of matrices can be expressed as $A\overrightarrow{x}=\overrightarrow{E}$ where $\overrightarrow{x}$ is any coordinate within the unit circle, $\overrightarrow{E}$ is the corresponding coordinate within the transformed elliptical space, and

$$A=\begin{bmatrix}r_{major}\cos\theta&-r_{minor}\sin\theta&D_x\\r_{major}\sin\theta&r_{minor}\cos\theta&D_y\\0&0&1\end{bmatrix}\tag{C2}$$

To find each point on the edge of the elliptical region, we use $\overrightarrow{x}\in\left\{\begin{bmatrix}x\\y\\1\end{bmatrix}\ni\begin{bmatrix}x\\y\\1\end{bmatrix}=\begin{bmatrix}\cos\phi\\\sin\phi\\1\end{bmatrix}\forall\,0\leq\phi\leq 2\pi\right\}$ and we find the equations for the edge of the rotated and displaced ellipse:

$$\forall\,0\leq\phi\leq 2\pi:$$

$$\begin{bmatrix}E_x(\phi)\\E_y(\phi)\end{bmatrix}=\begin{bmatrix}|r_{major}|\cos(\phi)\cos(\theta)-|r_{minor}|\sin(\phi)\sin(\theta)+D_x\\|r_{minor}|\sin(\phi)\cos(\theta)+|r_{major}|\cos(\phi)\sin(\theta)+D_y\end{bmatrix}\tag{C3}$$

Fig. C1 shows the rotated ellipse and the locations of the angles and measurements for these equations.

## References


Abatzoglou, J.T., 2013. Development of gridded surface meteorological data for ecological applications and modelling. Int. J. Climatol. 33, 121–131. https://doi.org/10.1002/joc.3413.

Abatzoglou, J.T., Brown, T.J., 2012. A comparison of statistical downscaling methods suited for wildfire applications. Int. J. Climatol. 32, 772–780. https://doi.org/10.1002/joc.2312.

Adair, E.C., Parton, W.J., Del Grosso, S.J., Silver, W.L., Harmon, M.E., Hall, S.A., Burke, I.C., Hart, S.C., 2008. Simple three-pool model accurately describes patterns of long-term litter decomposition in diverse climates. Glob. Chang. Biol. 14, 2636–2660. https://doi.org/10.1111/j.1365-2486.2008.01674.x.

Agee, J.K., 1996. The influence of forest structure on fire behavior. In: Proceedings of the 17th Annual Forest Vegetation Management Conference, pp. 52–68.

Arthur, M.A., Alexander, H.D., Dey, D.C., Schweitzer, C.J., Loftis, D.L., 2012. Refining the oak-fire hypothesis for management of oak-dominated forests of the eastern United States. J. Forestry 110, 257–266. https://doi.org/10.5849/jof.11-080.

Atchley, A.L., Linn, R., Jonko, A., Hoffman, C., Hyman, J.D., Pimont, F., Sieg, C., Middleton, R.S., 2021. Effects of fuel spatial distribution on wildland fire behaviour. Int. J. Wildland Fire 30, 179–189. https://doi.org/10.1071/WF20096.

Babl-Plauche, E.K., Alexander, H.D., Siegert, C.M., Willis, J.L., Berry, A.I., 2022. Mesophication of upland oak forests: implications of species-specific differences in leaf litter decomposition rates and fuelbed composition. For. Ecol. Manage. 512, 120141 https://doi.org/10.1016/j.foreco.2022.120141.

Berg, B., Lönn, M., 2022. Long-term effects of climate and litter chemistry on rates and stable fractions of decomposing scots pine and norway spruce needle litter—a synthesis. Forests 13, 125. https://doi.org/10.3390/f13010125.

Bright, B.C., Hudak, A.T., Meddens, A.J.H., Hawbaker, T.J., Briggs, J.S., Kennedy, R.E., 2017. Prediction of forest canopy and surface fuels from lidar and satellite time series data in a bark beetle-affected forest. Forests 8, 322. https://doi.org/10.3390/f8090322.

Campbell-Lochrie, Z., Walker-Ravena, C., Gallagher, M., Skowronski, N., Mueller, E.V., Hadden, R.M., 2021. Investigation of the role of bulk properties and in-bed structure in the flow regime of buoyancy-dominated flame spread in porous fuel beds. In: Fire Safety Journal, Fire Safety Science: Proceedings of the 13th International Symposium, 120, 103035. https://doi.org/10.1016/j.firesaf.2020.103035.

Carpenter, D.O., Taylor, M.K., Callaham, M.A., Hiers, J.K., Loudermilk, E.L., O'Brien, J.J., Wurzburger, N., 2020. Benefit or Liability? The ectomycorrhizal association may undermine tree adaptations to fire after long-term fire exclusion. Ecosystems. https://doi.org/10.1007/s10021-020-00568-7.

Coen, J.L., Schroeder, W., Conway, S., Tarnay, L., 2020. Computational modeling of extreme wildland fire events: a synthesis of scientific understanding with applications to forecasting, land management, and firefighter safety. J. Comput. Sci. 45, 101152 https://doi.org/10.1016/j.jocs.2020.101152.

Cornelissen, J.H.C., Grootemaat, S., Verheijen, L.M., Cornwell, W.K., van Bodegom, P.M., van der Wal, R., Aerts, R., 2017. Are litter decomposition and fire linked through plant species traits? New Phytol. 216, 653–669. https://doi.org/10.1111/nph.14766.

De Smedt, P., Wasof, S., Van de Weghe, T., Hermy, M., Bonte, D., Verheyen, K., 2018. Macro-detritivore identity and biomass along with moisture availability control forest leaf litter breakdown in a field experiment. Appl. Soil Ecol. 131, 47–54. https://doi.org/10.1016/j.apsoil.2018.07.010.

Dell, J.E., Richards, L.A., O'Brien, J.J., Loudermilk, E.L., Hudak, A.T., Pokswinski, S.M., Bright, B.C., Hiers, J.K., Williams, B.W., Dyer, L.A., 2017. Overstory-derived surface fuels mediate plant species diversity in frequently burned longleaf pine forests. Ecosphere 8, e01964. https://doi.org/10.1002/ecs2.1964.

Dupuy, J.-L., Linn, R.R., Konovalov, V., Pimont, F., Vega, J.A., Jiménez, E., 2011. Exploring three-dimensional coupled fire–atmosphere interactions downwind of wind-driven surface fires and their influence on backfires using the HIGRAD-FIRETEC model. Int. J. Wildland Fire 20, 734–750. https://doi.org/10.1071/WF10035.

Ferrari, J.B., Sugita, S., 1996. A spatially explicit model of leaf litter fall in hemlock–hardwood forests. Can. J. For. Res. 26, 1905–1913. https://doi.org/10.1139/x26-215.

Forrester, D.I., Bauhus, J., 2016. A review of processes behind diversity—productivity relationships in forests. Curr. Forestry Rep. 2, 45–61. https://doi.org/10.1007/s40725-016-0031-2.

Gajardo, J., García, M., Riaño, D., 2014. Applications of airborne laser scanning in forest fuel assessment and fire prevention. In: Maltamo, M., Næsset, E., Vauhkonen, J. (Eds.), Forestry Applications of Airborne Laser Scanning: Concepts and Case Studies, Eds. Springer, Netherlands, Dordrecht, pp. 439–462. https://doi.org/10.1007/978-94-017-8663-8_22.

García-Palacios, P., Shaw, E.A., Wall, D.H., Hättenschwiler, S., 2016. Temporal dynamics of biotic and abiotic drivers of litter decomposition. Ecol. Lett. 19, 554–563. https://doi.org/10.1111/ele.12590.

Gavazov, K.S., 2010. Dynamics of alpine plant litter decomposition in a changing climate. Plant Soil 337, 19–32. https://doi.org/10.1007/s11104-010-0477-0.

Goodwin, N.R., Coops, N.C., Culvenor, D.S., 2006. Assessment of forest structure with airborne LiDAR and the effects of platform altitude. Remote Sens. Environ. 103, 140–152. https://doi.org/10.1016/j.rse.2006.03.003.

Greene, D.F., Johnson, E.A., 1989. A model of wind dispersal of winged or plumed seeds. Ecology 70, 339–347. https://doi.org/10.2307/1937538.

Hawley, C.M., Loudermilk, E.L., Rowell, E.M., Pokswinski, S., 2018. A novel approach to fuel biomass sampling for 3D fuel characterization. MethodsX 5, 1597–1604. https://doi.org/10.1016/j.mex.2018.11.006.

Hiers, J.K., O'Brien, J.J., Mitchell, R.J., Grego, J.M., Loudermilk, E.L., 2009. The wildland fuel cell concept: an approach to characterize fine-scale variation in fuels and fire in frequently burned longleaf pine forests. Int. J. Wildland Fire 18, 315–325. https://doi.org/10.1071/WF08084.

Hiers, J.K., O'Brien, J.J., Will, R.E., Mitchell, R.J., 2007. Forest floor depth mediates understory vigor in xeric pinus palustris ecosystems. Ecol. Appl. 17, 806–814. https://doi.org/10.1890/06-1015.

Hoffman, C.M., Sieg, C.H., Linn, R.R., Mell, W., Parsons, R.A., Ziegler, J.P., Hiers, J.K., 2018. Advancing the science of wildland fire dynamics using process-based models. Fire 1, 32. https://doi.org/10.3390/fire1020032.

Hudak, A.T., Crookston, N.L., Evans, J.S., Hall, D.E., Falkowski, M.J., 2008. Nearest neighbor imputation of species-level, plot-scale forest structure attributes from LiDAR data. Remote Sens. Environ. Earth Observ. Terres. Biodiv. Ecosyst. Special Issue 112, 2232–2245. https://doi.org/10.1016/j.rse.2007.10.009.

Hyde, P., Dubayah, R., Walker, W., Blair, J.B., Hofton, M., Hunsaker, C., 2006. Mapping forest structure for wildlife habitat analysis using multi-sensor (LiDAR, SAR/InSAR, ETM+, Quickbird) synergy. Remote Sens. Environ. 102, 63–73. https://doi.org/10.1016/j.rse.2006.01.021.

Jarron, L.R., Coops, N.C., MacKenzie, W.H., Tompalski, P., Dykstra, P., 2020. Detection of sub-canopy forest structure using airborne LiDAR. Remote Sens. Environ. 244, 111770 https://doi.org/10.1016/j.rse.2020.111770.

Jonard, M., Andre, F., Ponette, Q., 2006. Modeling leaf dispersal in mixed hardwood forests using a ballistic approach. Ecology 87, 2306–2318. https://doi.org/10.1890/0012-9658(2006)87[2306:MLDIMH]2.0.CO;2.

Keane, R.E., 2008. Biophysical controls on surface fuel litterfall and decomposition in the northern Rocky Mountains, USA. Can. J. For. Res. 38, 1431–1445. https://doi.org/10.1139/X08-003.

Keane, R.E., Gray, K., Bacciu, V., Leirfallom, S., 2012. Spatial scaling of wildland fuels for six forest and rangeland ecosystems of the northern Rocky Mountains, USA. Landscape Ecol. 27, 1213–1234. https://doi.org/10.1007/s10980-012-9773-9.
Keane, R.E., Loehman, R.A., Holsinger, L.M., 2011. The FireBGCv2 landscape fire and succession model: a research simulation platform for exploring fire and vegetation dynamics. Gen. Tech. Rep. 137, 255. https://doi.org/10.2737/RMRS-GTR-255. RMRS-GTR-255. Fort Collins, CO: U.S. Department of Agriculture, Forest Service, Rocky Mountain Research Station.
Keane, R.E., Reeves, M., 2012. Use of expert knowledge to develop fuel maps for wildland fire management. In: Perera, A.H., Drew, C.A., Johnson, C.J. (Eds.), Expert Knowledge and Its Application in Landscape Ecology. Springer, New York, NY, pp. 211–228. https://doi.org/10.1007/978-1-4614-1034-8_11.
Koo, E., Linn, R.R., Pagni, P.J., Edminster, C.B., 2012. Modelling firebrand transport in wildfires using HIGRAD/FIRETEC. Int. J. Wildland Fire 21, 396–417. https://doi.org/10.1071/WF09146.
Lin, G., McCormack, M.L., Ma, C., Guo, D., 2017. Similar below-ground carbon cycling dynamics but contrasting modes of nitrogen cycling between arbuscular mycorrhizal and ectomycorrhizal forests. New Phytol. 213, 1440–1451. https://doi.org/10.1111/nph.14206.
Linn, R., Winterkamp, J., Colman, J.J., Edminster, C., Bailey, J.D., 2005. Modeling interactions between fire and atmosphere in discrete element fuel beds. Int. J. Wildland Fire 14, 37–48. https://doi.org/10.1071/WF04043.
Linn, R.R., Winterkamp, J.L., Furman, J.H., Williams, B., Hiers, J.K., Jonko, A., O'Brien, J.J., Yedinak, K.M., Goodrick, S., 2021. Modeling low intensity fires: lessons learned from 2012 RxCADRE. Atmosphere (Basel) 12, 139. https://doi.org/10.3390/atmos12020139.
Livneh, B., Rosenberg, E.A., Lin, C., Nijssen, B., Mishra, V., Andreadis, K.M., Maurer, E.P., Lettenmaier, D.P., 2013. A long-term hydrologically based dataset of land surface fluxes and states for the conterminous United States: update and extensions. J Clim 26, 9384–9392. https://doi.org/10.1175/JCLI-D-12-00508.1.
Loudermilk, E.L., Achtemeier, G.L., O'Brien, J.J., Hiers, J.K., Hornsby, B.S., 2014. High-resolution observations of combustion in heterogeneous surface fuels. Int. J. Wildland Fire 23, 1016–1026. https://doi.org/10.1071/WF13160.
Loudermilk, E.L., Cropper, W.P., Mitchell, R.J., Lee, H., 2011. Longleaf pine (Pinus palustris) and hardwood dynamics in a fire-maintained ecosystem: a simulation approach. Ecol. Modell. 222, 2733–2750. https://doi.org/10.1016/j.ecolmodel.2011.05.004.
Loudermilk, E.L., Hiers, J.K., O'Brien, J.J., 2017. The Role of Fuels for Understanding Fire Behavior and Fire Effects, in: Ecological Restoration and Management of Longleaf Pine Forests. CRC Press, pp. 107–122.
Loudermilk, E.L., Hiers, J.K., O'Brien, J.J., Mitchell, R.J., Singhania, A., Fernandez, J.C., Cropper, W.P., Slatton, K.C., 2009. Ground-based LIDAR: a novel approach to quantify fine-scale fuelbed characteristics. Int. J. Wildland Fire 18, 676–685. https://doi.org/10.1071/WF07138.
Midgley, M.G., Brzostek, E., Phillips, R.P., 2015. Decay rates of leaf litters from arbuscular mycorrhizal trees are more sensitive to soil effects than litters from ectomycorrhizal trees. J. Ecol. 103, 1454–1463. https://doi.org/10.1111/1365-2745.12467.
Mitchell, R.j., Marrs, R.h., Le Duc, M.g., Auld, M.h.d, 1999. A study of the restoration of heathland on successional sites: changes in vegetation and soil chemical properties. J. Appl. Ecol. 36, 770–783. https://doi.org/10.1046/j.1365-2664.1999.00443.x.
Mitchell, R.J., Hiers, J.K., O'Brien, J.J., Jack, S.B., Engstrom, R.T., 2006. Silviculture that sustains: the nexus between silviculture, frequent prescribed fire, and conservation of biodiversity in longleaf pine forests of the southeastern United States. Can. J. For. Res. 36, 2724–2736. https://doi.org/10.1139/x06-100.
Montgomery, R.A., Reich, P.B., Palik, B.J., 2010. Untangling positive and negative biotic interactions: views from above and below ground in a forest ecosystem. Ecology 91, 3641–3655. https://doi.org/10.1890/09-1663.1.
Mueller, E.V., Gallagher, M.R., Skowronski, N., Hadden, R.M., 2021. Approaches to modeling bed drag in pine forest litter for wildland fire applications. Transp. Porous Med. 138, 637–660. https://doi.org/10.1007/s11242-021-01637-8.
Nickmans, H., Jonard, M., Verheyen, K., Ponette, Q., 2019. Modelling leaf dispersal and nutrient return in tree species mixtures. For. Ecol. Manage. 436, 68–78. https://doi.org/10.1016/j.foreco.2019.01.001.
O'Brien, J.J., Loudermilk, E.L., Hiers, J.K., Pokswinski, S.M., Hornsby, B., Hudak, A.T., Strother, D., Rowell, E., Bright, B.C., 2016. Canopy-derived fuels drive patterns of in-fire energy release and understory plant mortality in a longleaf pine (Pinus palustris) sandhill in Northwest Florida, USA. Canad. J. Remote Sens. 42, 489–500. https://doi.org/10.1080/07038992.2016.1199271.
Olson, J.S., 1963. Energy storage and the balance of producers and decomposers in ecological systems. Ecology 44, 322–331. https://doi.org/10.2307/1932179.
Ottmar, R.D., Hiers, J.K., Butler, B.W., Clements, C.B., Dickinson, M.B., Hudak, A.T., O'Brien, J.J., Potter, B.E., Rowell, E.M., Strand, T.M., Zajkowski, T.J., 2015. Measurements, datasets and preliminary results from the RxCADRE project –2008, 2011 and 2012. Int. J. Wildland Fire 25, 1–9. https://doi.org/10.1071/WF14161.
Parsons, R.A., Linn, R.R., Pimont, F., Hoffman, C., Sauer, J., Winterkamp, J., Sieg, C.H., Jolly, W.M., 2017. Numerical investigation of aggregated fuel spatial pattern impacts on fire behavior. Land (Basel) 6, 43. https://doi.org/10.3390/land6020043.
Parsons, R.A., Pimont, F., Wells, L., Cohn, G., Jolly, W.M., de Coligny, F., Rigolot, E., Dupuy, J.-L., Mell, W., Linn, R.R., 2018. Modeling thinning effects on fire behavior with standfire. Ann. For. Sci. 75, 7. https://doi.org/10.1007/s13595-017-0686-2.
Pecot, S.D., Mitchell, R.J., Palik, B.J., Moser, E.B., Hiers, J.K., 2007. Competitive responses of seedlings and understory plants in longleaf pine woodlands: separating canopy influences above and below ground. Can. J. For. Res. 37, 634–648. https://doi.org/10.1139/X06-247.
Pimont, F., Parsons, R., Rigolot, E., de Coligny, F., Dupuy, J.-L., Dreyfus, P., Linn, R.R., 2016. Modeling fuels and fire effects in 3D: model description and applications. Environ. Modell. Softw. 80, 225–244. https://doi.org/10.1016/j.envsoft.2016.03.003.
Prescott, C.E., Grayston, S.J., 2013. Tree species influence on microbial communities in litter and soil: current knowledge and research needs. Forest Ecology and Management, Influence of tree species on forest soils. New Evid. Field Stud. 309, 19–27. https://doi.org/10.1016/j.foreco.2013.02.034.
Prior, L.D., Murphy, B.P., Bowman, D.M.J.S., 2018. Conceptualizing Ecological Flammability: an Experimental Test of Three Frameworks Using Various Types and Loads of Surface Fuels. Fire 1, 14. https://doi.org/10.3390/fire1010014.
Riegel, G.M., Miller, R.F., Krueger, W.C., 1992. Competition for resources between understory vegetation and overstory Pinus Ponderosa in Northeastern Oregon. Ecol. Appl. 2, 71–85. https://doi.org/10.2307/1941890.
Rothermel, R.C., 1972. A Mathematical Model For Predicting Fire Spread in Wildland Fuels, Research Paper INT-115. Intermountain Forest & Range Experiment Station. Forest Service, U.S. Department of Agriculture.
Rowell, E., Loudermilk, E.L., Hawley, C., Pokswinski, S., Seielstad, C., Queen, Ll., O'Brien, J.J., Hudak, A.T., Goodrick, S., Hiers, J.K., 2020. Coupling terrestrial laser scanning with 3D fuel biomass sampling for advancing wildland fuels characterization. For. Ecol. Manage. 462, 117945 https://doi.org/10.1016/j.foreco.2020.117945.
Ruiz, L.A., Hermosilla, T., Mauro, F., Godino, M., 2014. Analysis of the influence of plot size and LiDAR density on forest structure attribute estimates. Forests 5, 936–951. https://doi.org/10.3390/f5050936.
Scheller, R., Kretchun, A., Hawbaker, T.J., Henne, P.D., 2019. A landscape model of variable social-ecological fire regimes. Ecol. Modell. 401, 85–93. https://doi.org/10.1016/j.ecolmodel.2019.03.022.
Seielstad, C.A., Queen, L.P., 2003. Using airborne laser altimetry to determine fuel models for estimating fire behavior. J. Forestry 101, 10–15. https://doi.org/10.1093/jof/101.4.10.
Silva, C.A., Hudak, A.T., Vierling, L.A., Loudermilk, E.L., O'Brien, J.J., Hiers, J.K., Jack, S.B., Gonzalez-Benecke, C., Lee, H., Falkowski, M.J., Khosravipour, A., 2016. Imputation of individual longleaf pine (Pinus palustris Mill.) tree attributes from field and LiDAR data. Canad. J. Remote Sens. 42 (5), 554–573. https://doi.org/10.1080/07038992.2016.1196582, 42, 554–573.
Skowronski, N.S., Gallagher, M.R., Warner, T.A., 2020. Decomposing the interactions between fire severity and canopy fuel structure using multi-temporal, active, and passive remote sensing approaches. Fire 3, 7. https://doi.org/10.3390/fire3010007.
Staelens, J., Nachtergale, L., Luyssaert, S., Lust, N., 2003. A model of wind-influenced leaf litterfall in a mixed hardwood forest. Can. J. For. Res. 33, 201–209. https://doi.org/10.1139/x02-174.
Stephens, S.L., Finney, M.A., Schantz, H., 2004. Bulk density and fuel loads of ponderosa pine and white fir forest floors: impacts of leaf morphology. Northwest Sci. 78, 93–110.
Stoler, A.B., Relyea, R.A., 2011. Living in the litter: the influence of tree leaf litter on wetland communities. Oikos 120, 862–872. https://doi.org/10.1111/j.1600-0706.2010.18625.x.
Stowe, J., 2019. AFTER ACTION: witnessing drought in longleaf pine country. Wildfire Magaz. 4.
Tinkham, W.T., Smith, A.M.S., Hoffman, C., Hudak, A.T., Falkowski, M.J., Swanson, M.E., Gessler, P.E., 2012. Investigating the influence of LiDAR ground surface errors on the utility of derived forest inventories. Can. J. For. Res. 42, 413–422. https://doi.org/10.1139/x11-193.
Trap, J., Akpa-Vinceslas, M., Margerie, P., Boudsocq, S., Richard, F., Decaëns, T., Aubert, M., 2017. Slow decomposition of leaf litter from mature Fagus sylvatica trees promotes offspring nitrogen acquisition by interacting with ectomycorrhizal fungi. J. Ecol. 105, 528–539. https://doi.org/10.1111/1365-2745.12665.
Wade, D.D., Lunsford, J.D., 1989. A Guide for Prescribed Fire in Southern Forests. U.S. Department of Agriculture, Forest Service, Southern Region. Technical Publication R8-TP-11.